

Extraction and tracking method of drop zone of storm cells based on modified SCIT algorithms

X. Yu¹, X. Rui^{2*}, D. Zhang³, S. Yao¹, Y. Song¹, W. Sun⁴, L. Zhu⁵, L. Wu⁶

¹ School of Traffic and Transportation, Shijiazhuang Tiedao University, Shijiazhuang, China

² College of Resources and Environment, University of Chinese Academy of Sciences, Beijing, China

³ Baotou Meteorological Bureau, Baotou, China

⁴ The Third Institute of Surveying and Mapping of Hebei Province, Shijiazhuang, China

⁵ School of Geography Science, Nanjing Normal University, Nanjing, China

⁶ Anhui Weather Modification Office, Hefei, China

Received May 25, 2017; Revised July 20, 2017

In order to extract and to track the drop zone of storm cells under severe convection weather, a modified SCIT (Storm Cell Identification and Tracking) algorithm is proposed, and then, the coordinates (including longitude and latitude) of starting and ending positions of all segments in modified SCIT algorithm are calculated, based on these, the extraction and tracking methods of drop zones of storm cells on the ground are proposed to track and to simulate the precipitation processes. By using the raw weather radar data of CINRAD/CB type at Ordos city of China, one precipitation process in Central Region of Inner Mongolia on 31st July, 2014 afternoon are simulated and replayed, and the tracking results show that the proposed methods can locate and extract the probable precipitation belts precisely which play an important role in making out the precipitation forecast and precipitation assessment more accurately.

Key words: Modified SCIT algorithm, Drop zone of storm cells, Precipitation belts.

INTRODUCTION

If the accurate drop zones of active storm cells are obtained, the activity region of severe convection weather like hails can be accurately located too, and it can also meet the need of fine weather forecast in high resolution. The most well-known of storm cell identification and tracking algorithms include TITAN [1-3]. These algorithms attempt to decrease the dimensionality of the problem by first finding contiguous reflectivity values above a specific threshold along one-dimensional segments, grouping those segments to form two-dimensional components, and then grouping these two dimensional components to identify storm cells. Storm cells are then stored and identified by a centroid position or an ellipse with a shape, size, and orientation similar to that of the identified storm [1-2, 4]. But the exact shape of storm cell's drop zone cannot be fixed by these algorithms. Matthews and Trostel proposed an improved cell identification and tracking algorithm based on DBSCAN (short for Density-Based Spatial Clustering of Applications with Noise) clustering and JPDA (short for Joint Probabilistic Data Association) tracking methods, but they did not introduce the extraction methods of exact shape and the application of these in detail [4]. The occurrence of severe hail in China is not often, but

these are significant meteorological phenomena from the point of view of damage to agriculture, transportation and property. Hail events are limited in time and space, and the ground observation network can only provide partial information about the hail spatial distribution [5]. In order to solve these problem, an extraction and tracking method of drop zone of storm cells which can locate the exact drop zone of storm cells and track the storm cells for acquiring the movement direction was proposed, in the end, it was tested by raw data of CINRAD/CB radar in Ordos of city China.

PRINCIPLE OF THE MODIFIED SCIT ALGORITHMS

The storm cell is taken as a three-dimensional shape in SCIT algorithms, and the identification process of storm cell can be divided into three stages: (1) Searching the one-dimensional storm segments; (2) Combining the two-dimensional storm components; (3) Associating two or more components into three-dimensional storm cells vertically. It searches the storm segments which meet some certain conditions with 7 threshold values (The default values are 30, 35, 40, 45, 50, 55, 60 dBZ) on all radials of all cuts of raw data in the first stages. If neighboring segments at the same cuts are close to one another azimuthally and overlap in a range with a threshold value, then the segments are combined into storm components in

* To whom all correspondence should be sent:
E-mail: ruixpsz@163.com

As shown in Fig. 2, a radar station is located at Point A, with height h . Assuming the earth is a standard sphere, when a radar scanning ray with length r , and an elevation angle δ is sent from Point A to Point B, the length of BC is equal to $r \cos \delta$, and the length of OC is equal to $r \sin \delta + h + R_m$. Using the right angle $\angle OCB$, we can calculate the standard height, H , of Point B using Equation (4).

$$H = \sqrt{r^2 \cos^2 \delta + (r \sin \delta + h + R_m)^2} - R_m \quad (4)$$

Angle α and the arc length s from Fig. 2 can also be calculated as shown in equation (5) and equation (6):

$$\alpha = \arctan \frac{r \cos \delta}{r \sin \delta + h + R_m} \quad (5)$$

$$s = \frac{\alpha \pi R_m}{180} \quad (6)$$

In Fig. 2, if we know the longitude and latitude of Point A, the azimuth, and the spherical distance from Point A to Point B, the longitude and latitude of Point B can be calculated using the sine formula of spherical triangle and the cosine formula of spherical triangle [8].

In Fig. 2, longitude and latitude of point A are (λ_A, φ_A) , the longitude and latitude of Point B are (λ_B, φ_B) , and the azimuth from Point A to Point B is θ . Then the longitude and latitude of Points D and E are also (λ_A, φ_A) and (λ_B, φ_B) , and the azimuth from Point D to Point E is equal to θ in Fig. 3. Note that Point D and Point E are equivalent on Fig. 2 and Fig. 3. The North Pole is designated N, and the spherical distance from Point D to Point E is shown as s . We also save the spherical distance per 1° on the equator, and mark it by ΔS , its calculating formula is shown by equation (7).

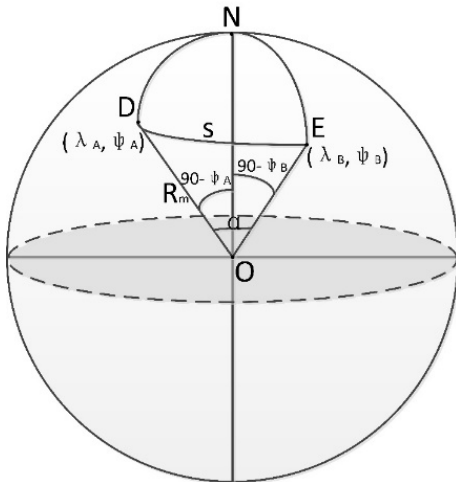


Fig. 3. Diagram for calculating longitude and latitude.

$$\Delta S = \frac{\pi R_m}{180} \quad (7)$$

Then angle $\angle DON$ is equal to $(90 - \varphi_A)$, and the spherical distance from Point D to Point N is equal to $(90 - \varphi_A) \times \Delta S$. While the angle $\angle NOE$ is equal to $(90 - \varphi_B)$, and the spherical distance from Point E to Point N is equal to $(90 - \varphi_B) \times \Delta S$. Since the spherical distance from Point D to Point E is equal to s , and the angle $\angle DOE$ is marked by α , then the three points D, N and E form a spherical triangle on the surface of the earth. According to the cosine formula of spherical triangle shown in equation (8):

$$\cos \angle NOE = \cos \angle NOD \cos \angle DOE + \sin \angle NOD \sin \angle DOE \cos \angle NDE \quad (8)$$

which corresponds to equation (9) and Equation (10):

$$\cos(90 - \varphi_B) = \cos(90 - \varphi_A) \cos \alpha + \sin(90 - \varphi_A) \sin \alpha \cos \theta \quad (9)$$

$$\sin \varphi_B = \sin \varphi_A \cos \alpha + \cos \varphi_A \sin \alpha \cos \theta \quad (10)$$

Which transforms to calculate the latitude of Point B, φ_B , as shown in equation (11).

$$\varphi_B = \arcsin(\sin \varphi_A \cos \alpha + \cos \varphi_A \sin \alpha \cos \theta) \quad (11)$$

According to the sine formula of spherical triangle, shown in equation (12):

$$\frac{\sin \angle DNE}{\sin \alpha} = \frac{\sin \angle NDE}{\sin(90 - \varphi_B)} = \frac{\sin \angle NED}{\sin(90 - \varphi_A)} \quad (12)$$

which transforms to equation (13):

$$\frac{\sin(\lambda_B - \lambda_A)}{\sin \alpha} = \frac{\sin \theta}{\sin(90 - \varphi_B)} = \frac{\sin \angle NED}{\sin(90 - \varphi_A)} \quad (13)$$

The longitude of Point B can be calculated after transforming to equation (14):

$$\lambda_B = \arcsin\left(\frac{\sin \alpha \sin \theta}{\sin(90 - \varphi_B)}\right) + \lambda_A \quad (14)$$

In Fig. 2, Point G is the blocking point during the visibility analysis between Point A and Point B. The GetLineofSight method of IGeoDatabaseBridge2 interface in ArcGIS Engine was used to calculate the longitude and latitude of Point G, which is equal to the longitude and latitude of Point J. This allows the angle $\angle DOJ$, β , to be calculated. From triangle $\triangle AFG$ and $\triangle OFG$, the length of AG can be derived from trigonometric functions and calculated using equation (15):

$$AG = \frac{\tan \beta \tan \delta (h + R_m)}{\sin \theta (1 - \tan \beta \tan \delta)} \quad (15)$$

We can calculate the coordinates (including longitude and latitude) of starting and ending positions of all segments by the above formulas.

After combining the segments into storm components by using the modified SCIT algorithms, one component will contain certain numbers of segments which are sorted by azimuth, and it is shown in Fig. 4. In this figure, we connect the starting points of segments to a line (marked by Line1) in a clockwise direction. In the same way,

we connect the ending points of segments to another line (marked by Line2). Then we connect the two lines to form a closed region which can be taken as the outline of this storm component.

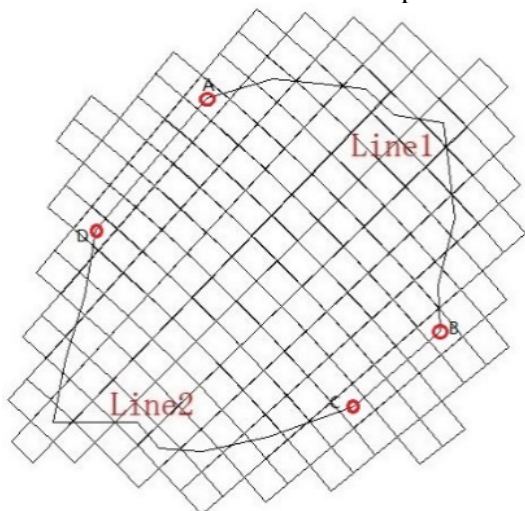


Fig. 4. Extraction of the outline of one component

During the connection, we create a List type of data structure which can save the starting point sets (marked by LstStartPnts) and the ending point sets (marked by LstEndPnts) of storm segments. If the points are saved into the list in a clockwise direction, we add the points in List LstEndPnts into the List LstStartPnts. After that, all the points of one closed storm components can be obtained. As the coordinates of these points saved in the list only include the longitude and latitude, the closed regions formed by these points are really the projection of storm components on the ground. By using this method, we can get all the projections on all cuts which can be used to form the drop zone of storm cells.

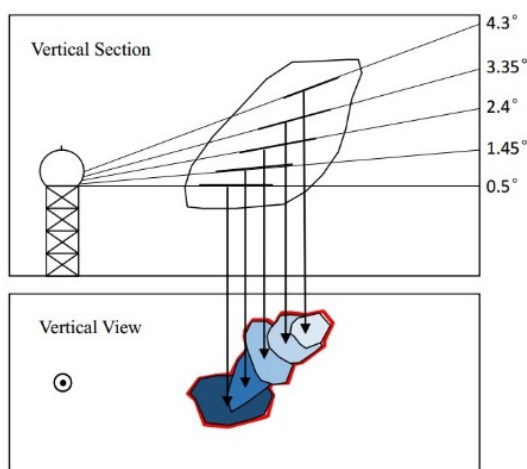


Fig. 5. Union operation of some components in one storm cell

As one storm cell contains two or more storm components which are relative in the vertical

direction, we can get the same number of projections of storm components which are saved in lists. Then we can unite the projections of storm components by using the Union operation of polygon-on-polygon-overlay tools in ArcGIS software. The final result of this operation will be the projections of storm cells on the ground, and it is also the drop zone of storm cells on the ground at this time, and it is shown in Fig. 5 marked by red line. At last, we extract the drop zones of all storm cells, and all the drop zones of storm cells scanned by the weather radar at this time can be obtained.

Tracking Method of Drop Zone of Storm Cells

As the storm cells are always moving on the echo maps at different scanning time, after the identification of storm cells, we need to track the storm cells according to the radar data at different time. This operation can be realized by using the modified SCIT algorithms further. As the storm cells move, the drop zones of storm cells move too, we need to track the drop zone for acquiring the accurate probable precipitation belts.

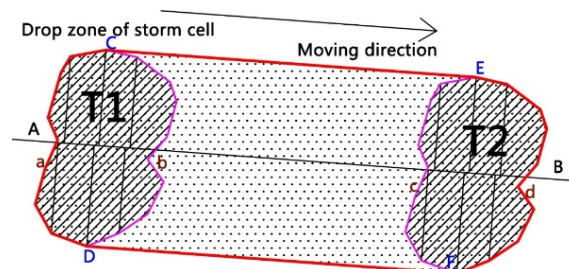


Fig. 6. Tracking method of Drop Zone of Storm Cells

In the above section, the drop zones of storm cells have been calculated accurately. In this section, we will introduce the tracking method of drop zones. In Fig. 6, we mark the drop zone of storm cells at the first observation time, whose color is carmine, by T1, and the drop zone at the second observation time is marked by T2. Supposing that the moving direction, which can be taken as the connection of centroid between polygon T1 and T2, is from A to B (marked by line AB), we draw the vertical lines from all the vertices of polygon T1 and T2 to line AB. The vertices (marked by C and E) corresponding to the two longest vertical lines above the line AB will be the vertices of the precipitation belts, in the same way, we can get the vertices D and F. The curve a is the left part of polygon T1 divided by vertices C and D, and curve d is the right part of polygon T2 divided by vertices E and F. Then the closed region formed by Line CE, Curve d, Line FD and Curve a will be the accurate probable precipitation belts between the observation time from T1 to T2.

By using the above method, the accurate probable precipitation belts for all the observation times can be acquired, based on this, and then we can make out the precipitation forecast and precipitation assessment more accurately.

TEST AND VERIFICATION OF THIS METHODS

Based on the above methods, we track and simulate one precipitation process in Central Region of Inner Mongolia on July 31, 2014 afternoon (Beijing Time, similarly hereinafter) by using the raw radar data scanned at 18:56. The identified storm cells by using the modified SCIT algorithms at different threshold values (including 35dBZ, 40dBZ and 45dBZ) are shown in Fig. 7, 8 and 9.

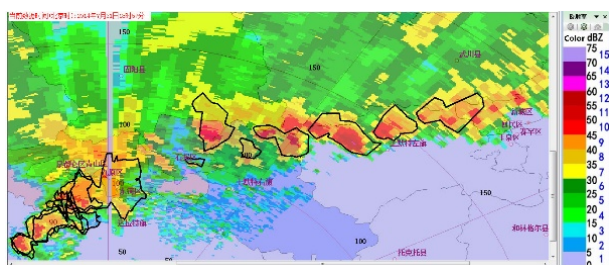


Fig. 7. Identified storm cells by using the modified SCIT algorithms at 35dBZ

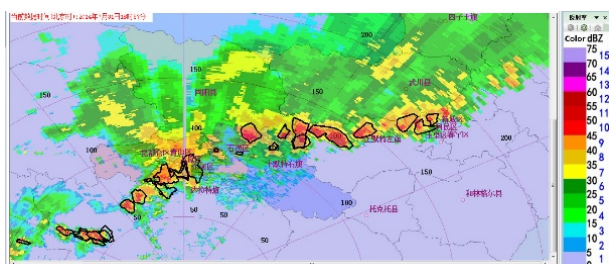


Fig. 8. Identified storm cells by using the modified SCIT algorithms at 40dBZ

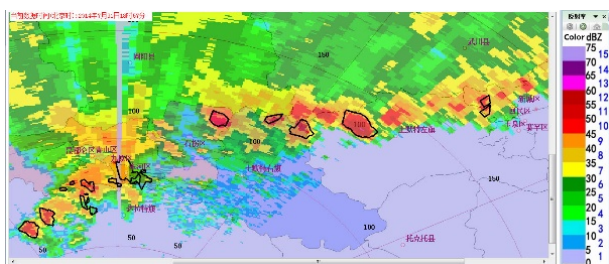


Fig. 9. Identified storm cells by using the modified SCIT algorithms at 45dBZ

The identification results of storm cells at different observation time are shown in one map, and it is shown in Fig. 10. From this figure, we can know that the storm cells are moving to east-southeast direction. Then the storm cell identification and tracking results are analyzed. From this results, we can locate the drop zone and the passing region of storm cells, besides, the

results have certain instructive effect on forecasting and estimating the amount of precipitation and the precipitation intensity.

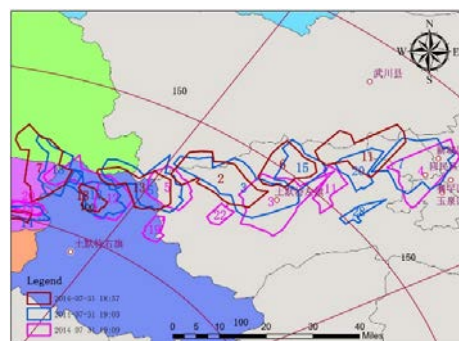


Fig. 10. Tracking results of storm cells at different observation time

CONCLUSIONS AND DISCUSSIONS

A modified SCIT algorithms proposed by the authors is introduced firstly in this paper, based on the algorithms, and then the extraction and tracking methods of drop zones of storm cells on the ground are proposed to track and to simulate the precipitation processes. By using the raw weather radar data of CINRAD/CB type at Ordos city of China, one precipitation process in Central Region of Inner Mongolia on July 31, 2014 afternoon are simulated and replayed, and the tracking results show that the proposed methods can locate and extract the probable precipitation belts precisely which play an important role in making out the precipitation forecast and precipitation assessment more accurately. In this paper, we just tracked and simulated the precipitation belts, not including the hail-fall area. If the hail detection algorithms are added into these methods and the hail-fall area can be calculated out in the future, it will have more significance for forecasting the hail-fall area and appraising the damage caused by hailstorms more accurately.

Acknowledgements: The research reported herein was sponsored by the National Science and Technology Major Project of China (Grant No. 2011ZX05039-004), the National Science and Technology Support Program of China (Grant No. 2012BAC25B01), the National Natural Science Foundation of China (Grant No. 51308358), the Hebei Province Natural Science Fund (Grant No. D2016210008) and the Social Science Foundation Project of Hebei Province (Grant No. HB15SH015).

REFERENCES

1. M. Dixon, G. Wiener, *Journal of Atmospheric and Oceanic Technology*, **10**(6), 785 (1993).
2. J.T. Johnson, P.L. MacKeen, A. Witt, E.D.W. Mitchell, G.J. Stumpf, M.D. Eilts, K. W. Thomas, *Weather and Forecasting*, **13**(2), 263 (1998).
3. L. Han, S. Fu, L. Zhao, Y. Zheng, H. Wang, Y. Lin, *Journal of Atmospheric and Oceanic Technology*, **26**(4), 719 (2009).
4. J. Matthews, J. Trostel, in: An Improved Storm Cell Identification and Tracking (SCIT) Algorithm based on DBSCAN and JPDA Tracking Methods (Proc. 26th Conference on Interactive Information and Processing Systems (IIPS) for Meteorology, Oceanography, and Hydrology, Orlando, 2010), Orlando, 2010, p. 1.
5. K. Skripniková, D. Řezáčová, *Atmospheric Research*, **144**(0), 175 (2014).
6. J. Bech, B. Codina, J. Lorente, D. Bebbington, in: Anomalous Propagation Effects on Weather Radar Beam Blockage Corrections (Proc. 30th International Conference on Radar Meteorology, Munich, 2001), Munich, 2001, p. 267.
7. J. Bech, B. Codina, J. Lorente, D. Bebbington, *Journal of Atmospheric and Oceanic Technology*, **20**(6), 845 (2003).
8. Y. Wan, , H. Yang, Y. Xiao, C. Wu, X. Xu, *Quarterly Journal of Applied Meteorology*, **11**(4), 440 (2000).